Matter

Article

Self-sustaining reactive species program morphological evolution across timescales in hydrogels

Graphical abstract

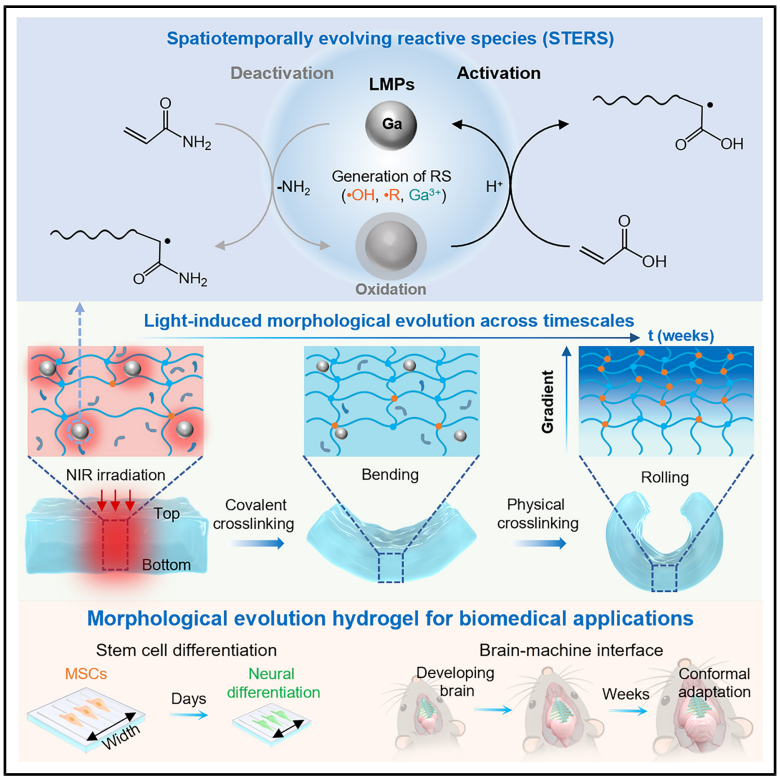

Highlights

- Life-like, self-sustaining STERS generation maintained for up to 4 weeks
- NIR light-mediated spatiotemporal reactive species gradients for programmed gelation
- Hydrogel morphological evolution spanning micro- to macro-scales and minutes to weeks
- Novel evolving hydrogel-based devices for dynamical biomedical scenarios

Authors

Mingzhe Nie, Mingxing Peng, Xun Li, Weizhong Xu, Jiachuan Hua, Massimiliano Galluzzi, Xuemin Du

Correspondence

xm.du@siat.ac.cn

In brief

We report a life-like, self-sustaining system for generating spatiotemporally evolving reactive species (STERS) based on vinyl monomer-mediated activation and deactivation of gallium-based liquid metal particles (LMPs). This STERS system enables programmable morphological evolution in hydrogels across micro- to macro-scales and over minutes to weeks. We demonstrate the utility of these morphology-evolving hydrogels in adaptive biomedical applications, including directing stem cell differentiation toward osteogenic and neural lineages over days, and monitoring EEG signals in the developing brain over weeks.

Nie et al., 2026, Matter 9, 103004
December 2, 2026
https://doi.org/10.1016/j.matt.2026.103004

CellPress

Please cite this article in press as: Nie et al., Self-sustaining reactive species program morphological evolution across timescales in hydrogels, Matter (2026), https://doi.org/10.1016/j.matt.2026.103004

Matter

CellPress

Article

Self-sustaining reactive species program morphological evolution across timescales in hydrogels

Mingzhe Nie,[1] Mingxing Peng,[1] Xun Li,[2] Weizhong Xu,[1] Jiachuan Hua,[1] Massimiliano Galluzzi,[2] and Xuemin Du[1,3,*]
[1]State Key Laboratory of Biomedical Imaging Science and System, Center for Intelligent Biomedical Materials and Devices (IBMD), Shenzhen Institutes of Advanced Technology (SIAT), Chinese Academy of Sciences (CAS), Shenzhen 518055, P.R. China
[2]Institute of Advanced Materials Science and Engineering, Shenzhen Institutes of Advanced Technology (SIAT), Chinese Academy of Sciences (CAS), Shenzhen 518055, P.R. China
[3]Lead contact
*Correspondence: xm.du@siat.ac.cn
https://doi.org/10.1016/j.matt.2026.103004

PROGRESS AND POTENTIAL Morphological evolution in living systems—from the rapid nastic movements of plant leaves to the gradual sculpting of animal tissues—arises from the sustained production and spatial organization of active chemical species. However, current shape-morphing polymers cannot fully recapitulate biological morphodynamics because they lack the self-sustaining, life-like generation of spatiotemporally evolving reactive species (STERS). Here, we report a biological morphodynamics-inspired strategy that enables self-sustaining STERS generation, thereby programming hydrogel morphological evolution across timescales. The STERS system integrates three key components: gallium-based liquid metal particles (LMPs) that generate reactive species, classical vinyl monomers that react with LMPs, and near-infrared (NIR) light that establishes spatiotemporal gradients of reactive species. Through synergistic interactions, the system generates and maintains concentration gradients of reactive species (radicals and ions) for up to 4 weeks after a single NIR exposure, continuously initiating free radical polymerization and ionic complexation to progressively establish evolving crosslinking gradients. This approach enables programmable, life-like morphological evolution in hydrogels across microscopic to macroscopic scales, from minutes to weeks, and through single and multiple shape-morphing cycles. We further extend these morphology-evolving hydrogels to biomedical applications, including directing stem cell differentiation toward osteogenic and neural lineages over days, and monitoring electroencephalogram (EEG) signals in the developing brain over weeks. These findings suggest that STERS and morphology-evolving hydrogels offer a promising platform for next-generation intelligent materials and devices, with broad implications for robotics, regenerative medicine, and brain-machine interfaces.

SUMMARY

Morphological evolution across multiple timescales, sustained by spatiotemporally evolving reactive species (STERS), underpins living systems' development and adaptation. However, synthetic materials rarely recapitulate such evolving morphodynamics. Here, we propose a novel strategy that enables life-like generation of STERS, programming hydrogel morphological evolution across micro- to macro-scales and over minutes to weeks. This STERS system integrates gallium-based liquid metal particles, vinyl monomers, and near-infrared (NIR) light to establish spatiotemporal reactive species gradients for weeks following a single NIR exposure. STERS drive progressive free radical polymerization and ionic complexation, generating spatiotemporally evolving crosslinking gradients and enabling programmable shape transformations. We further extend these morphology-evolving hydrogels to biomedical applications, including directing stem cell differentiation and monitoring electroencephalogram signals in the developing brain. These advances pave the way for a new paradigm in the design of next-generation intelligent materials and devices, with promising applications in robotics, regenerative medicine, and brain-machine interfaces.

Please cite this article in press as: Nie et al., Self-sustaining reactive species program morphological evolution across timescales in hydrogels, Matter (2026), https://doi.org/10.1016/j.matt.2026.103004

INTRODUCTION

Morphological evolution in living systems—from the rapid nastic movements of plant leaves to the gradual sculpting of animal tissues—arises from the sustained production and spatial organization of active chemical species. These species orchestrate diffusion, reaction, and feedback processes, thereby coordinating morphology transformations across timescales spanning seconds to weeks.[1–6] For example, young sunflower plants exhibit heliotropic bending throughout the day by continuously generating and spatially establishing auxin concentration gradients across the illuminated and shaded sides of the stem, which induces differential cell elongation and directional growth.[7,8] By contrast, most synthetic stimulus-responsive polymers are fully polymerized materials whose shape transformations depend on stimulus-induced network reconfiguration, typically mediated by dynamic covalent exchange or reversible noncovalent interactions, and are thus limited to rapid and transient responses on timescales of seconds to minutes.[9–21] Temporal programming strategies have extended the duration of network reconfiguration in polymers by leveraging mechanisms such as supramolecular interactions,[22,23] autocatalytic networks,[24,25] and controlled mass diffusion,[26] thereby prolonging shape transformations to hours or days. However, current shape-morphing polymers still cannot recapitulate the morphodynamics observed in biological systems, as they lack the self-sustaining generation of spatiotemporally evolving reactive species (STERS) required to program morphogenesis across timescales. This mechanism gap restricts the realization of life-like morphological evolution, thereby constraining their practical applications in biomedical scenarios that require operation across specific biological life cycle.[2,5,27–32]

Here, we report a biological morphodynamics-inspired strategy that enables life-like, self-sustaining generation of STERS, thereby programming morphological evolution across timescales in hydrogels. The STERS system comprises three essential components: gallium-based liquid metal particles (LMPs) that generate reactive species, classical vinyl monomers (acrylamide [AAm] and acrylic acid [AAc]) that react with LMPs, and near-infrared (NIR) light to establish spatiotemporal gradients of reactive species (Figures 1A and 1B). Through synergistic interactions, the STERS system generates and maintains concentration gradients of reactive species (radicals and ions) for up to 4 weeks following a single NIR exposure, continuously initiating free radical polymerization and ionic complexation to progressively establish spatiotemporally evolving crosslinking gradients. This novel approach enables programmable, life-like morphological evolution in hydrogels, spanning microscopic to macroscopic scales, minutes to weeks, and single to multiple transformation cycles. We further demonstrate the utility of these morphology-evolving hydrogels in biomedical applications, including directing stem cell differentiation into osteogenic and neural lineages in a life-like cycle, and monitoring electroencephalogram (EEG) signals in the developing brain (postnatal day 14 [P14]–P28). These advances pave the way for a new paradigm in designing next-generation intelligent materials and devices, with promising applications in robotics, regenerative medicine, and brain-machine interfaces.

RESULTS AND DISCUSSION

Sustained generation of reactive species

To achieve self-sustaining generation of reactive species, we designed the STERS system based on three key criteria: (1) the functional element must dynamically switch between the deactivation and activation states, enabling controlled production of reactive species; (2) conventional monomers should facilitate both deactivation and activation reactions of the functional element, thus regulating the generation of reactive species and the formation of polymer network; and (3) the system should be compatible with an external field to convert external energy into spatiotemporal gradients of reactive species. To meet these requirements (Figures 1A and 1B), we employed gallium-based LMPs as the functional element, leveraging their unique ability to generate reactive species (e.g., radicals and Ga^{3+} ions) through surface oxide formation and removal,[33,34] thereby enabling dynamic deactivation and activation reactions. We selected classical vinyl monomers, including AAm and AAc, which interact with the oxide layer of LMPs and can be polymerized into various functional materials.[35–39] As the external field, we utilized 808-nm NIR light, which is applicable for biomedical applications,[40–43] offers high spatial resolution, and can be efficiently coupled with LMPs to convert NIR irradiation into localized thermal energy.[44–47]

On the basis of this design principle, we first synthesized LMPs and then prepared a well-dispersed hydrogel precursor containing LMPs, AAm, AAc, and poly (ethylene glycol) diacrylate (PEGDA) as the crosslinker (Figure S1, see supplemental methods). Before NIR irradiation, the LMPs underwent repeated cycles of oxide formation and removal within the precursor, rapidly converting the solution into a pre-gel matrix. During these dynamic deactivation and activation reactions, AAm binds more strongly to the oxide surface than to the underlying Ga surface, stabilizing the oxide layer and facilitating Ga^{3+} outward diffusion, thereby promoting the oxide growth,[33] whereas AAc preferentially etches the oxide layer of the LMPs,[48,49] as confirmed by transmission electron microscopy (TEM) and energy-dispersive X-ray spectroscopy (EDS) (Figure 1A; Figures S2–S4). These reactions sustained the generation of reactive species (·OH, ·R, and Ga^{3+}), as evidenced by electron paramagnetic resonance (EPR) spectroscopy and inductively coupled plasma mass spectrometry (ICP-MS), respectively (Figures S5 and S6). Specifically, radical species originated from the oxidation reactions between Ga and water in the presence of oxygen, while Ga^{3+} ions were generated through reactions between the gallium oxide layer and protons from the system.[35,50] Unlike conventional approaches, in which reactions typically proceed to completion almost instantaneously,[51–53] this self-sustaining system, enabled by unique dynamic deactivation and activation reactions, can persist for over 4 weeks without external chemical replenishment and can be further regulated by NIR irradiation.

Upon exposure of the pre-gel matrix to NIR irradiation, the well-dispersed LMPs efficiently converted incident energy into localized thermal gradients, thereby accelerating interfacial reactions and facilitating the generation of reactive species (Figure 1B). Notably, a single NIR irradiation event triggered the spatiotemporal evolution of reactive species within the pre-gel matrix, as confirmed by fluorescence image analysis (Figures S7 and S8).

Please cite this article in press as: Nie et al., Self-sustaining reactive species program morphological evolution across timescales in hydrogels, Matter (2026), https://doi.org/10.1016/j.matt.2026.103004

CellPress

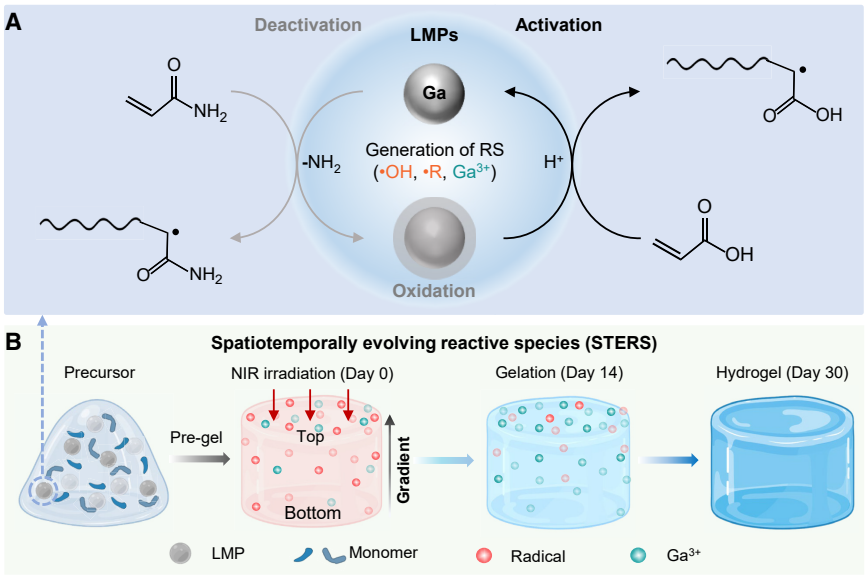

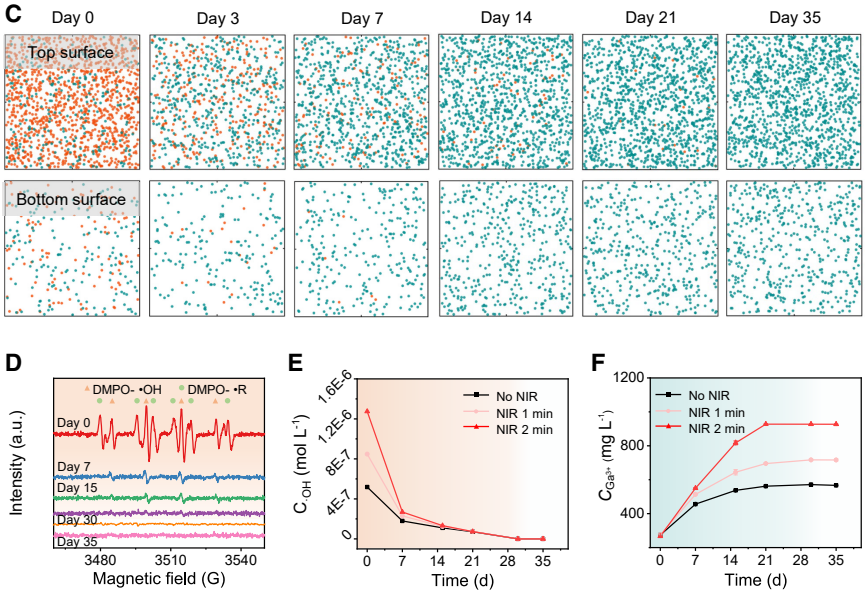

Figure 1. Spatiotemporal evolution of reactive species

(A) Schematic of the design and principle of the STERS system.

(B) Schematics for the self-sustaining generation of spatiotemporally evolving reactive species (RS, radicals and ions) for up to 4 weeks following a single NIR exposure.

(C) Fluorescence image analysis demonstrating that a single NIR irradiation (808 nm, 2 W cm^{-2}, 1 min) induces spatiotemporal concentration gradients of radicals (orange dots) and Ga^{3+} ions (blue dots) within the pre-gel matrix.

(D) EPR spectra of hydroxyl radical and alkyl radical generated in the STERS system (NIR 1 min) from day 0 to day 35.

(E) Time-dependent generation of ·OH in the STERS system (no NIR, NIR 1 min, and NIR 2 min) from day 0 to day 35.

(F) Time-dependent generation of Ga^{3+} in the STERS system (no NIR, NIR 1 min, and NIR 2 min) from day 0 to day 35.

As shown in Figure 1C, the concentration of radical species was significantly higher at the top surface than at the bottom surface on day 0, and this difference gradually diminished over time until no significant difference remained by day 21. In contrast, Ga^{3+} release was initially low on both surfaces on day 0, with only a modest difference between them, but gradually increased over time and peaked at the top surface on day 21 before leveling off. These results indicate that NIR irradiation establishes the spatiotemporal concentration gradients of reactive species within the pre-gel matrix, ascribed to the enhanced dynamic deactivation/activation reactions and NIR light attenuation through the film thickness.[16,54] Furthermore, the spatiotemporal evolution of reactive species was highly dependent on both the LMP concentration and the NIR irradiation duration (Figures 1D–1F; Figures S9–S11). By optimizing the LMP concentration (10.71 wt %) and NIR irradiation duration (1 min), the radical concentration reached approximately 8.48×10^{-7} M on day 0, with sustained generation up to 21 days (day 21: approximately 7.46×10^{-8} M, Figures 1D and 1E). Similarly, Ga^{3+} generation persisted for 21 days, reaching approximately 717 mg L^{-1} on day 30 (Figure 1F). Collectively, these results demonstrate that by kinetically modulating the deactivation and activation reactions, the STERS system enables life-like, self-sustaining generation of reactive species, with spatiotemporal concentrations sufficient to induce further gelation.[55]

Light-induced spatiotemporal gelation

We next investigated the light-induced spatiotemporal gelation process. Upon NIR irradiation, the LMPs embedded within the pre-gel film rapidly absorbed NIR energy, leading to localized temperature increases (Figure S12). This photothermal effect resulted in concentration gradients of reactive species, thereby inducing spatiotemporal gelation (Figure 2A). As the LMPs were progressively consumed during the generation of radical species and Ga^{3+} ions, the residual monomers in the pre-gel film underwent polymerization and crosslinking, forming both covalently and physically crosslinked networks. As shown in Figure 2B, both the size and number of LMPs decreased markedly by day 15 and were nearly depleted by day 30, relative to day 0, consistent with their sustained generation of reactive species. Correspondingly, AAm and AAc underwent polymerization, as shown in Figures 2C and S13. At the initial stage (day 0), AAc polymerization was dominant because of the strongly acidic precursor

Please cite this article in press as: Nie et al., Self-sustaining reactive species program morphological evolution across timescales in hydrogels, Matter (2026), https://doi.org/10.1016/j.matt.2026.103004

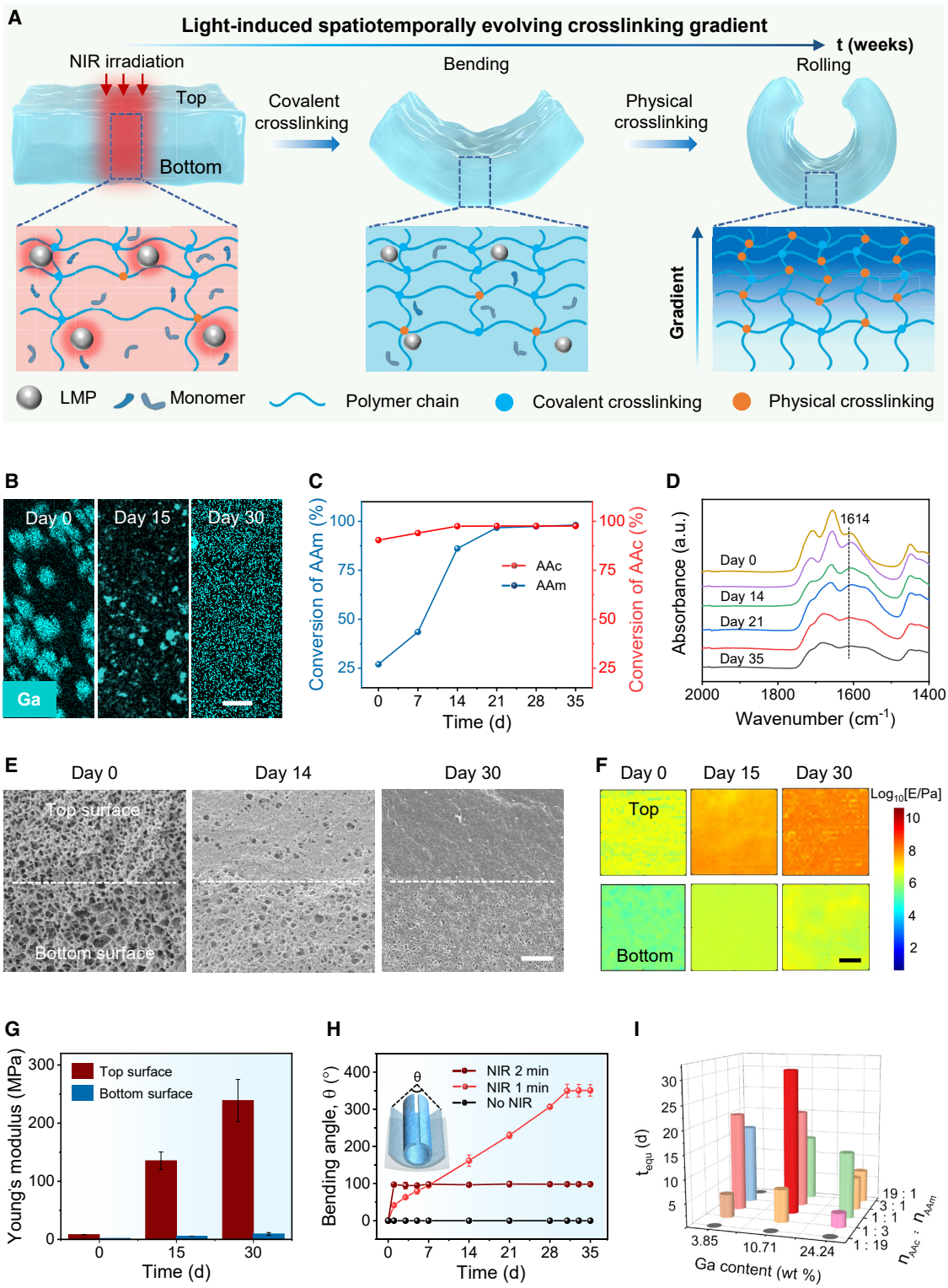

Figure 2. Light-induced spatiotemporal gelation

(A) Schematic for the progressive establishment of spatiotemporally evolving crosslinking gradients, including covalently and physically crosslinked networks, induced by light.

(B) EDS mapping showing LMP consumption within the hydrogel film after a single NIR irradiation (808 nm, 2 W cm^{-2}, 1 min). Scale bars: 10 μm.

(C) Monomer conversion rates of AAm and AAc from day 0 to day 35.

(legend continued on next page)

Please cite this article in press as: Nie et al., Self-sustaining reactive species program morphological evolution across timescales in hydrogels, Matter (2026), https://doi.org/10.1016/j.matt.2026.103004

environment, in which AAc remained largely undissociated and, thus, more reactive, whereas AAm was protonated and became less reactive, as reported previously.[56,57] By day 14, the monomer conversions of both AAm and AAc exceeded ~90%, indicating that covalent crosslinking had become the predominant process during this period. Notably, Fourier transform infrared (FTIR) spectra revealed a new absorption band at 1,614 cm^{-1} after 14 days (Figure 2D; Figure S14), attributable to the coordination interactions between carboxyl groups and Ga^{3+} ions,[50] suggesting that physical crosslinks became predominant at the later stage. Together, these results demonstrate that NIR irradiation induces the sequential formation of covalently and physically crosslinked networks within the hydrogel. Moreover, fluorescence imaging confirmed the presence of NIR light-induced spatiotemporally evolving crosslinking gradients within the hydrogel (Figure S15).

This evolving crosslinking density gradient was further confirmed by scanning electron microscopy (SEM) analysis. As shown in Figures 2E and S16, the hydrogel film initially exhibited a uniform porous structure. After NIR irradiation, however, the pore sizes at the top surface decreased markedly, whereas the bottom surface largely retained its original morphology. These results indicate a more densely crosslinked polymer network at the top and a looser network at the bottom. Notably, the crosslinking density gradient persisted for over 4 weeks after a single NIR irradiation. An additional line of evidence for the light-induced spatiotemporal crosslinking density gradient was provided by atomic force microscopy (AFM) mapping of Young's modulus (Figure 2F). Before NIR irradiation, Young's modulus values were similar at both the top and bottom surfaces and increased gradually over 4 weeks (Figures S17A and S17B). After NIR irradiation, the Young's modulus at the top surface increased sharply from 8.31 ± 0.03 MPa on day 0 to 135.37 ± 15 MPa on day 15 and 238.93 ± 36.3 MPa on day 30, indicating progressive stiffening of the hydrogel network (Figures 2F and 2G). In contrast, the bottom surface showed only a modest increase, from 1.84 ± 0.00 MPa on day 0 to 5.6 ± 0.01 MPa on day 15 and 9.47 ± 2.33 MPa on day 30, reflecting a comparatively softer network structure. The modulus difference could be further increased by extending the NIR irradiation duration (Figures S17C and S17D).

Notably, this light-induced crosslinking density gradient resulted in differential swelling across the film thickness, producing out-of-plane stress and consequently causing bending toward the irradiation direction.[58–60] The bending angle could be modulated by adjusting the irradiation duration and film thickness (Figure 2H; Figures S18 and 19). Remarkably, this morphological evolution persisted for up to 4 weeks, and its duration could be tuned by varying the irradiation duration, LMP concentration, or monomer ratio (Figure 2I; Figures S20–S22). Importantly, this strategy is also applicable to diverse monomers (Figure S23), as various functional groups can interact with LMPs.[33] Collectively, these results indicate that hydrogel morphological evolution can be modulated over timescales ranging from minutes to weeks, a capability not achievable in conventional fully polymerized systems.

Multiscale morphological evolution

We next investigated programmable morphological evolution in hydrogels. To begin, a structural color hydrogel film with a butterfly motif, embedded with highly ordered polystyrene (PS) colloidal crystals, exhibited progressive color changes over extended timescales. As shown in Figure 3A, a PS colloidal crystal film was first assembled and then infused with the hydrogel precursor (see supplemental methods). The progressive gelation process increased the crosslinking density of the structural color hydrogel film, thereby gradually decreasing the lattice spacing of the colloidal crystal structure (Figure S24), as evidenced by visible color changes and corresponding shifts in the reflectance spectra. Figure 3B shows that the structural color of the butterfly motif evolved from red to green over 1 month, with the reflection peak blue shifting from 617 to 568 nm. Such evolving structural coloration not only provides a vivid, real-time indicator of gelation progress across a month-long timescale but also mimics biological morphodynamics at the microscale.[61]

Beyond microscale morphological evolution, the incorporation of patterned NIR irradiation during gelation enables programmable macroscale shape transformation of hydrogels. For example, directing NIR light through a 45°-angled grating induced a helical deformation of an initially planar hydrogel sheet. As shown in Figure 3C, the flat film (day 1) progressively twisted into a helix by day 5, reached equilibrium after 30 days, and became transparent by day 35, consistent with the gradual consumption of LMPs (Figure 2B). Notably, immersion in ethylene diamine tetraacetic acid (EDTA) solution competitively chelated Ga^{3+} ions from physical crosslinking sites, reducing network density and reversibly restoring the original day-1 morphology (Figures 3C and 3D), in agreement with the gelation process. Extending this strategy, a mushroom-shaped arched film subjected to patterned illumination gradually flattened over 14 days and stabilized by day 28, mimicking the growth dynamics of natural mushrooms (Figure 3E; Figure S25). Importantly, site-specific pre-gel irradiation enabled reliable and reversible morphological reprogramming. As illustrated in Figure 3F, a flat star-shaped pre-gel film underwent sequential bending at five neck regions (sites 1–5) upon localized NIR irradiation along the thickness direction, generating crosslinking gradients. Subsequent irradiation from the opposite side erased these gradients and restored

(D) FTIR spectra of the hydrogel film after a single NIR irradiation (1 min) from day 0 to day 35.
(E) SEM images showing the evolution of cross-sectional morphology of the hydrogel film after a single NIR irradiation (1 min) from day 0 to day 14 to day 30. Scale bars: 10 μm.
(F) Young's modulus mapping of the top and bottom surfaces of the hydrogel film after a single NIR irradiation (1 min) from day 0 to day 15 to day 30. Scale bars: 2.5 μm.
(G) Young's modulus of both the top and bottom surfaces of the hydrogel film increases from day 0 to day 15 and to day 30 after a single NIR irradiation (1 min).
(H) Evolution of the bending dynamics in hydrogel sheets under different NIR irradiation conditions (no NIR, 1 min, and 2 min) over 5 weeks.
(I) Phase diagram illustrating the morphological evolution of hydrogel sheets as a function of irradiation duration, LMP concentration, and monomer ratio.

Please cite this article in press as: Nie et al., Self-sustaining reactive species program morphological evolution across timescales in hydrogels, Matter (2026), https://doi.org/10.1016/j.matt.2026.103004

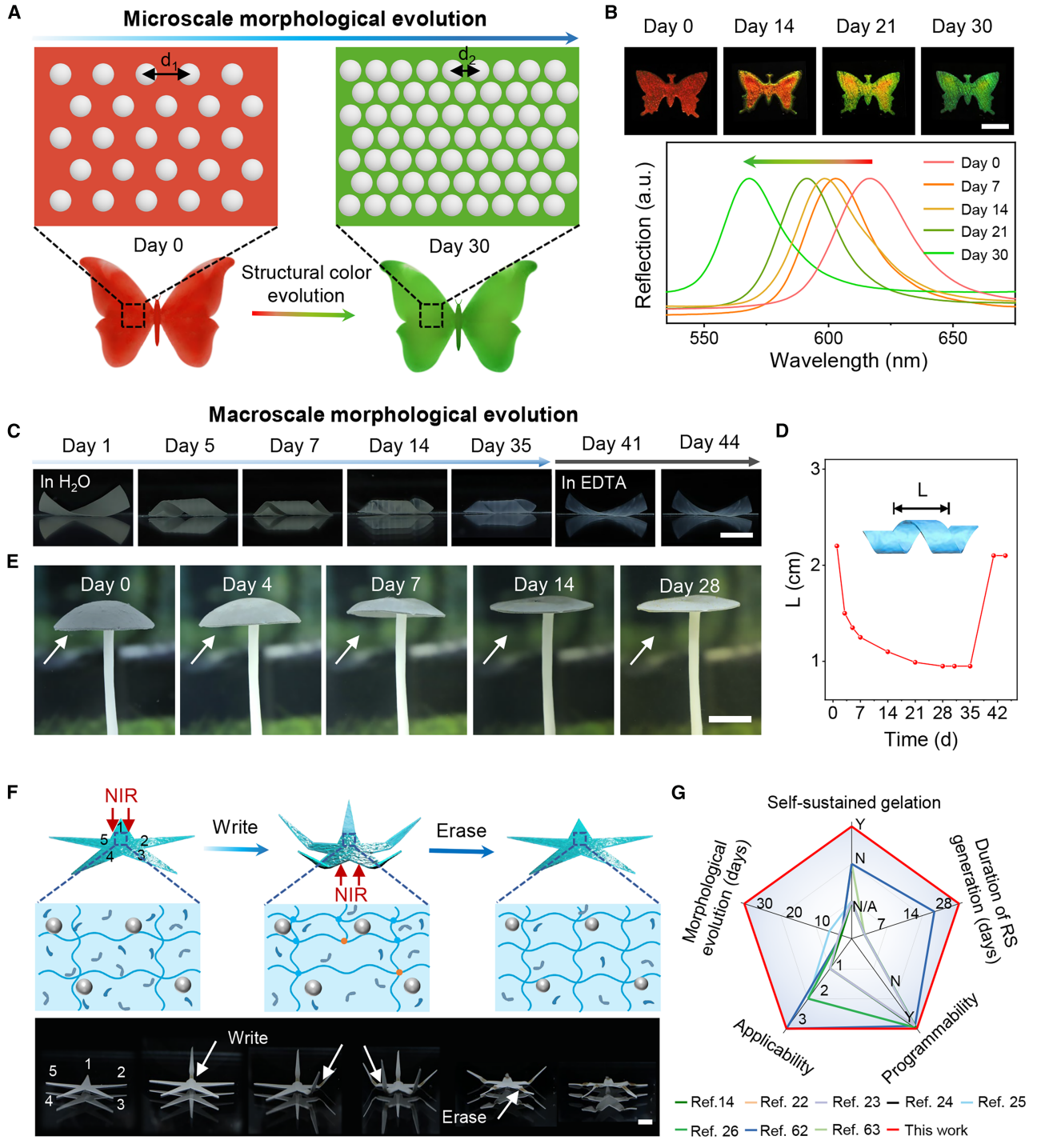

Figure 3. Multiscale morphological evolution

(A) Schematic for the evolving structural coloration of a butterfly-motif hydrogel film, resulting from the decreased lattice spacing (d_1–d_2) of the PS colloidal crystal structures.

(B) Structural color change of the butterfly-motif hydrogel film from initial red to final green over 1 month, accompanied by blue-shifted reflection peaks. Scale bars: 500 μm.

(C and D) NIR irradiation (2 W cm^{-2}, 1 min) through a 45°-angled grating induces a helical transformation of a planar hydrogel sheet from day 0 to day 44. Scale bars: 1 cm.

(legend continued on next page)

Please cite this article in press as: Nie et al., Self-sustaining reactive species program morphological evolution across timescales in hydrogels, Matter (2026), https://doi.org/10.1016/j.matt.2026.103004

the flat configuration, allowing repeated cycles of light-written and light-erased deformation (Figure S26). Compared with previous strategies, this approach offered distinct advantages, including self-sustained reactive species generation and gelation, morphological evolution spanning timescales from minutes to a month, high programmability, and superior compatibility to various monomers (Figure 3G; Table S1).[14,22–26,62,63] These features provide new opportunities for morphological evolutional hydrogels in biomedical domains that require operation across specific biological lifecycles.

Diverse biomedical applications

Directional differentiation of stem cells is essential for engineering complex tissues, such as neural and bone constructs, and critically depends on the precise regulation of biochemical and biophysical cues within a dynamically evolving cellular microenvironment.[2,44,64,65] However, conventional materials generally provide static biomechanical cues and lack the spatiotemporal adaptability required to recapitulate such dynamic conditions, thereby limiting their effectiveness in guiding stem cell fate. To address this limitation, we developed a light-induced evolutional platform (Evol-P) capable of microscale morphological evolution, enabling the regulation of stem cell differentiation through dynamic topographical cues. As illustrated in Figures 4A and 4B and Figure S27, Evol-P was fabricated by encapsulating a morphology-evolving hydrogel (Evol-gel) film between two pre-prepared polydimethylsiloxane (PDMS) films, one bearing microgrooves on its surface, followed by 1 min of NIR irradiation and subsequent seeding of mesenchymal stem cells (MSCs) (see supplemental methods). This platform provided a biocompatible and dynamic microenvironment that allowed remote and precise modulation of MSC differentiation (Figures S28 and S29). In the absence of NIR irradiation, the internal width of the static microgroove structures (control) remained constant at 9.8 μm, promoting osteogenic differentiation, as evidenced by increased Runx2 expression (Figure S30). After a single NIR exposure, the microgroove width in the evolutional platform (Evol-P1) gradually decreased from 9.8 to 9.2 μm over 6 days, still favoring osteogenic differentiation but with slightly reduced Runx2 expression (Figures 4C and 4E). Notably, a second NIR irradiation applied after 3 days of culture further reduced the microgroove width to 8.7 μm (Evol-P2), which effectively promoted neural differentiation, as indicated by increased Tuj-1 expression and decreased Runx2 expression (Figures 4D and 4E). These results demonstrate that the spatiotemporally evolving platform, enabled by adaptive microscale topographical modulation, provides a dynamic biomechanical environment with great potential for tissue engineering and next-generation intelligent biomedical devices.[66,67]

Besides, bioelectronic devices for recording or stimulating neural activity hold significant promise for treating neurological disorders.[32,45,68,69] However, conventional bioelectronics, typically characterized by fixed morphologies, cannot accommodate the dynamic growth of biological tissues. This mismatch may lead to interfacial signal loss, necessitate additional surgical interventions, and increase the risk of complications.[29,70–72] To overcome these limitations, we developed macroscale shape-evolving bioelectronics (Evol-E) by integrating a PDMS-encapsulated shape-evolving hydrogel onto flexible electrode arrays with 30 channels, enabling chronic monitoring of EEG signal evolution in the growing skull of 2-week-old rats (P14) (see supplemental methods). During development, the skull surface undergoes pronounced morphological changes (Figure 4F), accompanied by substantial variations in neuronal number, maturation, and network connectivity, which can be visualized through neural network mapping. As shown in Figures 4G–4I, both Evol-E and control electrodes exhibited comparable neural network complexity and connectivity at P14, as both conformed well to the relatively flat brain surface at this stage. By P21, neural network mapping revealed increased complexity and connectivity in the Evol-E group compared with controls, as evidenced by a greater number of connections between nodes (Figure 4J). This improvement is attributed to the dynamically evolving morphology of Evol-E, which enables spatiotemporal adaptation to growing brain (Figure S31). Notably, by P28, the Evol-E group demonstrated a marked increase in both total connections and connected nodes, surpassing the control group due to superior morphological conformity between the device and the developing brain (Figures S31–S37). These findings were further supported by the synchronization score mapping, which showed enhanced and dominated γ, θ, and β band activities, indicative of neural circuit maturation (Figures 4H and 4I; Figures S32–S34). Collectively, these results demonstrate that shape-evolving bioelectronics can conform to the developing neural tissue, enabling more accurate neural signal mapping and providing a novel strategy for studying brain function evolution and developing dynamically adaptive brain-machine interfaces.[45,73]

Conclusions

In summary, we report a new strategy for kinetically modulating the vinyl monomer-mediated deactivation and activation reactions of gallium-based LMPs, enabling life-like, self-sustained generation of STERS to program hydrogel morphological evolution across multiple timescales. This STERS system sustains concentration gradients of reactive species (radicals and ions) for up to 4 weeks following a single NIR exposure, enabling continuous free radical polymerization and ionic complexation that progressively establish spatiotemporally evolving crosslinking gradients within the hydrogel networks. Notably, this innovative strategy enables programmable, life-like morphological evolution of hydrogels spanning microscopic to macroscopic scales, minutes to weeks, and single to multiple transformation cycles. We further extend these morphology-evolving hydrogels to biomedical applications, including directing stem cell

(E) Mimicking the natural growth dynamics of a mushroom by exposing a mushroom-shaped arched hydrogel film to patterned NIR irradiation (2 W cm^{-2}, 1 min). Scale bars: 1 cm.

(F) Sequential bending of a flat star-shaped pre-gel film at five neck positions (sites 1–5) upon precise NIR targeting along the thickness direction. Scale bars: 0.5 cm.

(G) Comparison of shape-morphing hydrogels between this work and previously reported studies across five criteria. Y, yes; N, no; NG, not given.

Please cite this article in press as: Nie et al., Self-sustaining reactive species program morphological evolution across timescales in hydrogels, Matter (2026), https://doi.org/10.1016/j.matt.2026.103004

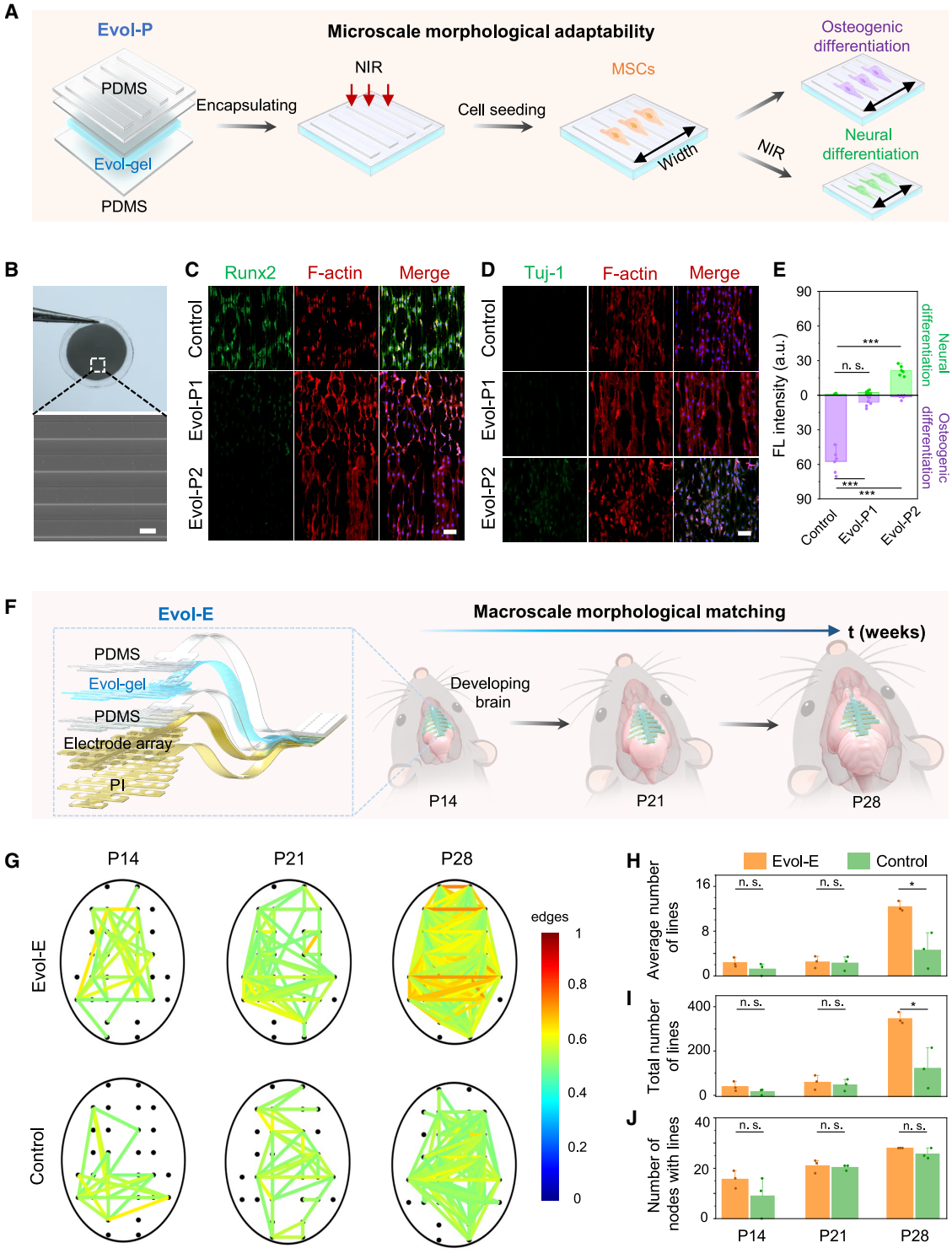

Figure 4. Diverse biomedical applications

(A) Schematic of the light-induced evolutional platform (Evol-P) with microscale morphological adaptability for directing stem cell differentiation.

(B) Photography of Evol-P and SEM image showing its surface morphology. Scale bars: 10 μm.

(C) Fluorescence images showing the osteogenic differentiation of MSCs on control device, Evol-P1 (single NIR irradiation), and Evol-P2 (twice NIR irradiation). Scale bars: 100 μm.

(D) Fluorescence images showing neural differentiation of MSCs on control device, Evol-P1, and Evol-P2. Scale bars: 100 μm.

(legend continued on next page)

differentiation toward osteogenic and neural lineages over days, and monitoring EEG signals in the developing brain over weeks. These findings highlight that STERS and morphology-evolving hydrogels offer a transformative strategy for developing next-generation intelligent materials and devices, with broad implications for robotics, regenerative medicine, and brain-machine interfaces.

METHODS

Further details regarding the methods can be found in the supplemental methods.

RESOURCE AVAILABILITY

Lead contact

All queries about experimental procedures can be directed to the lead contact, Xuemin Du (xm.du@siat.ac.cn).

Materials availability

All relevant vendors and preparation procedures are included in supplemental information files. All unique reagents generated in this study are available from the lead contact, with a completed material(s) transfer agreement.

Data and code availability

This study did not generate any datasets.

ACKNOWLEDGMENTS

The authors acknowledge the financial support provided by the National Natural Science Foundation of China (52022102 and 52261160380), the Youth Innovation Promotion Association of CAS (Y2023100), the Fundamental Research Program of Shenzhen (RCJC20221008092729033, JCYJ20220818101800001, and JCYJ20230807140608017), and the Shenzhen Medical Research Fund (B2302045). The authors also thank Dr. Qilong Zhao for his help in biological experiments, preparing the supplementary materials, and inspiring discussion.

AUTHOR CONTRIBUTIONS

X.D. conceived the idea and designed the experiments in discussion with M.N.; M.N. conducted the experiments with assistance from M.P., W.X., and J.H.; X.L. and M.G. performed Young's modulus analysis with AFM; X.D. analyzed the results and wrote the manuscript with output from M.N. All authors contributed to the discussion and interpretation of the results.

DECLARATION OF INTERESTS

The authors declare no competing interests.

SUPPLEMENTAL INFORMATION

Supplemental information can be found online at https://doi.org/10.1016/j.matt.2026.103004.

Received: April 26, 2026
Revised: July 16, 2026
Accepted: August 8, 2026

REFERENCES

1. Hogan, B.L.M. (1999). Morphogenesis. Cell *96*, 225–233. https://doi.org/10.1016/s0092-8674(00)80562-0.
2. Cadart, C., Venkova, L., Recho, P., Lagomarsino, M.C., and Piel, M. (2019). The physics of cell-size regulation across timescales. Nat. Phys. *15*, 993–1004. https://doi.org/10.1038/s41567-019-0629-y.
3. Scepanovic, G., and Fernandez-Gonzalez, R. (2024). Should I shrink or should I grow: cell size changes in tissue morphogenesis. Genome *67*, 125–138. https://doi.org/10.1139/gen-2023-0091.
4. Guo, Q., Dai, E., Han, X., Xie, S., Chao, E., and Chen, Z. (2015). Fast nastic motion of plants and bioinspired structures. J. R. Soc. Interface *12*, 20150598. https://doi.org/10.1098/rsif.2015.0598.
5. Quan, H., Kisailus, D., and Meyers, M.A. (2020). Hydration-induced reversible deformation of biological materials. Nat. Rev. Mater. *6*, 264–283. https://doi.org/10.1038/s41578-020-00251-2.
6. Zhang, F., Yang, M., Xu, X., Liu, X., Liu, H., Jiang, L., and Wang, S. (2022). Unperceivable motion mimicking hygroscopic geometric reshaping of pine cones. Nat. Mater. *21*, 1357–1365. https://doi.org/10.1038/s41563-022-01391-2.
7. Atamian, H.S., Creux, N.M., Brown, R.I., Garner, A.G., Blackman, B.K., and Harmer, S.L. (2016). Circadian regulation of sunflower heliotropism, floral orientation, and pollinator visits. Science *353*, 587–590. https://doi.org/10.1126/science.aaf9793.
8. Brooks, C.J., Atamian, H.S., and Harmer, S.L. (2023). Multiple light signaling pathways control solar tracking in sunflowers. PLoS Biol. *21*, e3002344. https://doi.org/10.1371/journal.pbio.3002344.
9. Ni, C., Chen, D., Wen, X., Jin, B., He, Y., Xie, T., and Zhao, Q. (2023). High speed underwater hydrogel robots with programmable motions powered by light. Nat. Commun. *14*, 7672. https://doi.org/10.1038/s41467-023-43576-6.
10. Lv, J.-a., Liu, Y., Wei, J., Chen, E., Qin, L., and Yu, Y. (2016). Photocontrol of fluid slugs in liquid crystal polymer microactuators. Nature *537*, 179–184. https://doi.org/10.1038/nature19344.
11. Guo, K., Yang, X., Zhou, C., and Li, C. (2024). Self-regulated reversal deformation and locomotion of structurally homogenous hydrogels subjected to constant light illumination. Nat. Commun. *15*, 1694. https://doi.org/10.1038/s41467-024-46100-6.
12. Liu, J., Huang, Y.-S., Liu, Y., Zhang, D., Koynov, K., Butt, H.-J., and Wu, S. (2024). Reconfiguring hydrogel assemblies using a photocontrolled

(E) Quantitative analysis of fluorescence intensity for Runx2 (osteogenic marker) and Tuj-1 (neuronal marker). Runx2: Evol-P1 vs. control, $p < 0.001$ (***) and Evol-P2 vs. control, $p < 0.001$ (***); $n = 6$ separate experiments; Tuj-1: Evol-P1 vs. control, $p = 0.050$ (n.s.) and Evol-P2 vs. control, $p < 0.001$ (***); $n = 6$ separate experiments.
(F) Schematic illustration of Evol-E used for EEG recording from the skull of 2-week-old neonatal rats from P14 to P28.
(G) Neural network mapping for the γ band (connections with a threshold > 0.5) during rat development from P14 to P28.
(H) Average number of connected lines. P14: control vs. Evol-E, $p = 0.232$ (n.s.); P21: control vs. Evol-E, $p = 0.845$ (n. s.); P28: control vs. Evol-E, $p = 0.044$ (*). $n = 3$ rats.
(I) Total number of connected lines. P14: control vs. Evol-E, $p = 0.212$ (n.s.); P21: control vs. Evol-E, $p = 0.648$ (n.s.); P28: control vs. Evol-E, $p = 0.043$ (*). $n = 3$ rats.
(J) Number of nodes with lines for γ band at P14, P21, and P28 recorded by Evol-E or control electrodes. P14: control vs. Evol-E: $p = 0.294$ (n.s.); P21: control vs. Evol-E, $p = 0.718$ (n.s.); P28: control vs. Evol-E, $p = 0.192$ (n.s.). $n = 3$ rats.
Statistical comparisons for the data shown in (E), (H), (I), and (J) were performed using one-way ANOVA with two-tailed Student's t test.

metallopolymer adhesive for multiple customized functions. Nat. Chem. *16*, 1024–1033. https://doi.org/10.1038/s41557-024-01476-2.

13. Fan, W., Shan, C., Guo, H., Sang, J., Wang, R., Zheng, R., Sui, K., and Nie, Z. (2019). Dual-gradient enabled ultrafast biomimetic snapping of hydrogel materials. Sci. Adv. *5*, eaav7174. https://doi.org/10.1126/sciadv.aav7174.
14. Zhu, Q.L., Du, C., Dai, Y., Daab, M., Matejdes, M., Breu, J., Hong, W., Zheng, Q., and Wu, Z.L. (2020). Light-steered locomotion of muscle-like hydrogel by self-coordinated shape change and friction modulation. Nat. Commun. *11*, 5166. https://doi.org/10.1038/s41467-020-18801-1.
15. He, X., Aizenberg, M., Kuksenok, O., Zarzar, L.D., Shastri, A., Balazs, A.C., and Aizenberg, J. (2012). Synthetic homeostatic materials with chemo-mechano-chemical self-regulation. Nature *487*, 214–218. https://doi.org/10.1038/nature11223.
16. Hu, H., Nie, M., Galluzzi, M., Yu, X., and Du, X. (2023). Mimosa-inspired high-sensitive and multi-responsive starch actuators. Adv. Funct. Mater. *33*, 2304634. https://doi.org/10.1002/adfm.202304634.
17. Wang, Y., Cui, H., Zhao, Q., and Du, X. (2019). Chameleon-inspired structural-color actuators. Matter *1*, 626–638. https://doi.org/10.1016/j.matt.2019.05.012.
18. Zhang, L., Naumov, P., Du, X., Hu, Z., and Wang, J. (2017). Vapomechanically responsive motion of microchannel-programmed actuators. Adv. Mater. *29*, 1702231. https://doi.org/10.1002/adma.201702231.
19. Wang, S., Gao, Y., Wei, A., Xiao, P., Liang, Y., Lu, W., Chen, C., Zhang, C., Yang, G., Yao, H., and Chen, T. (2020). Asymmetric elastoplasticity of stacked graphene assembly actualizes programmable untethered soft robotics. Nat. Commun. *11*, 4359. https://doi.org/10.1038/s41467-020-18214-0.
20. Jeon, S.-J., Hauser, A.W., and Hayward, R.C. (2017). Shape-morphing materials from stimuli-responsive hydrogel hybrids. Acc. Chem. Res. *50*, 161–169. https://doi.org/10.1021/acs.accounts.6b00570.
21. Xia, X., Spadaccini, C.M., and Greer, J.R. (2022). Responsive materials architected in space and time. Nat. Rev. Mater. *7*, 683–701. https://doi.org/10.1038/s41578-022-00450-z.
22. Hu, X., Zhou, J., Vatankhah-Varnosfaderani, M., Daniel, W.F.M., Li, Q., Zhushma, A.P., Dobrynin, A.V., and Sheiko, S.S. (2016). Programming temporal shapeshifting. Nat. Commun. *7*, 12919. https://doi.org/10.1038/ncomms12919.
23. Peng, W., Zhang, G., Zhao, Q., and Xie, T. (2021). Autonomous off-equilibrium morphing pathways of a supramolecular shape-memory polymer. Adv. Mater. *33*, 2102473. https://doi.org/10.1002/adma.202102473.
24. Paikar, A., Novichkov, A.I., Hanopolskyi, A.I., Smaliak, V.A., Sui, X., Kampf, N., Skorb, E.V., and Semenov, S.N. (2022). Spatiotemporal regulation of hydrogel actuators by autocatalytic reaction networks. Adv. Mater. *34*, 2106816. https://doi.org/10.1002/adma.202106816.
25. Fusi, G., Del Giudice, D., Skarsetz, O., Di Stefano, S., and Walther, A. (2023). Autonomous soft robots empowered by chemical reaction networks. Adv. Mater. *35*, 2209870. https://doi.org/10.1002/adma.202209870.
26. Ni, C., Chen, D., Yin, Y., Wen, X., Chen, X., Yang, C., Chen, G., Sun, Z., Wen, J., Jiao, Y., et al. (2023). Shape memory polymer with programmable recovery onset. Nature *622*, 748–753. https://doi.org/10.1038/s41586-023-06520-8.
27. Zhang, Y.S., and Khademhosseini, A. (2017). Advances in engineering hydrogels. Science *356*, eaaf3627. https://doi.org/10.1126/science.aaf3627.
28. Vaia, R., and Baur, J. (2008). Adaptive composites. Science *319*, 420–421. https://doi.org/10.1126/science.1152931.
29. Tang, X., Shen, H., Zhao, S., Li, N., and Liu, J. (2023). Flexible brain-computer interfaces. Nat. Electron. *6*, 109–118. https://doi.org/10.1038/s41928-022-00913-9.
30. Lee, Y.B., Jeon, O., Lee, S.J., Ding, A., Wells, D., and Alsberg, E. (2021). Induction of four-dimensional spatiotemporal geometric transformations in high cell density tissues via shape-changing hydrogels. Adv. Funct. Mater. *31*, 2010104. https://doi.org/10.1002/adfm.202010104.
31. Eftekhari, B.S., Eskandari, M., Janmey, P.A., Samadikuchaksaraei, A., and Gholipourmalekabadi, M. (2020). Surface topography and electrical signaling: Single and synergistic effects on neural differentiation of stem cells. Adv. Funct. Mater. *30*, 1907792. https://doi.org/10.1002/adfm.201907792.
32. Liu, Y., Li, J., Song, S., Kang, J., Tsao, Y., Chen, S., Mottini, V., McConnell, K., Xu, W., Zheng, Y.-Q., et al. (2020). Morphing electronics enable neuromodulation in growing tissue. Nat. Biotechnol. *38*, 1031–1036. https://doi.org/10.1038/s41587-020-0495-2.
33. Castilla-Amorós, L., Chien, T.-C.C., Pankhurst, J.R., and Buonsanti, R. (2022). Modulating the reactivity of liquid Ga nanoparticle inks by modifying their surface chemistry. J. Am. Chem. Soc. *144*, 1993–2001. https://doi.org/10.1021/jacs.1c12880.
34. Ma, J., Krisnadi, F., Vong, M.H., Kong, M., Awartani, O.M., and Dickey, M.D. (2023). Shaping a soft future: Patterning liquid metals. Adv. Mater. *35*, 2205196. https://doi.org/10.1002/adma.202205196.
35. Ma, J., Lin, Y., Kim, Y.-W., Ko, Y., Kim, J., Oh, K.H., Sun, J.-Y., Gorman, C.B., Voinov, M.A., Smirnov, A.I., et al. (2019). Liquid metal nanoparticles as initiators for radical polymerization of vinyl monomers. ACS Macro Lett. *8*, 1522–1527. https://doi.org/10.1021/acsmacrolett.9b00783.
36. Gan, T., Handschuh-Wang, S., Shang, W., Shen, J., Zhu, L., Xiao, Q., Hu, S., and Zhou, X. (2019). Liquid metal-mediated mechanochemical polymerization. Macromol. Rapid Commun. *40*, 1900537. https://doi.org/10.1002/marc.201900537.
37. Shang, Y., Huang, C., Li, Z., and Du, X. (2025). Bioinspired ultra-stretchable and highly sensitive structural color electronic skins. Adv. Funct. Mater. *35*, 2412703. https://doi.org/10.1002/adfm.202412703.
38. Peng, Y., Xin, Y., Zhang, J., Dickey, M.D., and Li, Q. (2023). Functional heterophasic liquid metals. Responsive Mater. *1*, e20230003. https://doi.org/10.1002/rpm.20230003.
39. Jaseem, S.A., Rahmani, P., Sakorikar, T., Ma, J., Almutairi, O., Voinov, M.A., Smirnov, A.I., Chen, B., and Dickey, M.D. (2026). Liquid metals as initiators of free-radical polymerization of hydrogels: A perspective. Adv. Funct. Mater. *36*, e14024. https://doi.org/10.1002/adfm.202514024.
40. Bassam, A., Du, M., Li, Y., and He, X. (2025). Engineering in NIR-responsive photothermal materials and their application in wound healing administration. Responsive Mater. *3*, e20240031. https://doi.org/10.1002/rpm.20240031.
41. Xu, Y., Tang, Y., and Li, Q. (2025). Visible- and near-infrared light-driven molecular photoswitches for biological applications. Adv. Funct. Mater. *35*, 2416359. https://doi.org/10.1002/adfm.202416359.
42. Luo, J.Q., Xu, J.K., Bisoyi, H.K., Xue, Z.Y., Qiu, W.Q., Tang, J.S., Lu, H.F., Tang, Y., and Li, Q. (2026). High-performance flexible pyroelectric energy harvesting system enabled by light-driven thermomechanical coupling in liquid crystal elastomer. Adv. Mater. *38*, e19065. https://doi.org/10.1002/adma.202519065.
43. Wang, F., Liu, M., Liu, C., Huang, C., Zhang, L., Cui, A., Hu, Z., and Du, X. (2023). Light control of droplets on photo-induced charged surfaces. Natl. Sci. Rev. *10*, nwac164. https://doi.org/10.1093/nsr/nwac164.
44. Peng, M., Zhao, Q., Chai, A., Wang, Y., Wang, M., and Du, X. (2025). A ferroelectric living interface for fine-tuned exosome secretion toward physiology-mimetic neurovascular remodeling. Matter *8*, 101901. https://doi.org/10.1016/j.matt.2024.10.019.
45. Wang, F., Wang, L., Zhu, X., Lu, Y., and Du, X. (2025). Neuron-Inspired Ferroelectric Bioelectronics for Adaptive Biointerfacing. Adv. Mater. *37*, 2416698. https://doi.org/10.1002/adma.202416698.
46. Wang, F., Liu, M., Liu, C., Zhao, Q., Wang, T., Wang, Z., and Du, X. (2022). Light-induced charged slippery surfaces. Sci. Adv. *8*, eabp9369. https://doi.org/10.1126/sciadv.abp9369.
47. Wang, F., Liu, C., Dai, Z., Xu, W., Ma, X., Gao, Y., Ge, X., Zheng, W., and Du, X. (2025). Photopyroelectric tweezers for versatile manipulation. Innovation *6*, 100742. https://doi.org/10.1016/j.xinn.2024.100742.

48. Lee, G.-H., Lee, D.H., Jeon, W., Yoon, J., Ahn, K., Nam, K.S., Kim, M., Kim, J.K., Koo, Y.H., Joo, J., et al. (2023). Conductance stable and mechanically durable bi-layer EGaIn composite-coated stretchable fiber for 1D bioelectronics. Nat. Commun. *14*, 4173. https://doi.org/10.1038/s41467-023-39928-x.

49. Lee, D.H., Lim, T., Pyeon, J., Park, H., Lee, S.W., Lee, S., Kim, W., Kim, M., Lee, J.C., Kim, D.W., et al. (2024). Self-mixed biphasic liquid metal composite with ultra-high stretchability and strain-insensitivity for neuromorphic circuits. Adv. Mater. *36*, 2310956. https://doi.org/10.1002/adma.202310956.

50. Xu, J., Wang, Z., You, J., Li, X., Li, M., Wu, X., and Li, C. (2020). Polymerization of moldable self-healing hydrogel with liquid metal nanodroplets for flexible strain-sensing devices. Chem. Eng. J. *392*, 123788. https://doi.org/10.1016/j.cej.2019.123788.

51. Li, G., Zhang, M., Liu, S., Yuan, M., Wu, J., Yu, M., Teng, L., Xu, Z., Guo, J., Li, G., et al. (2023). Three-dimensional flexible electronics using solidified liquid metal with regulated plasticity. Nat. Electron. *6*, 154–163. https://doi.org/10.1038/s41928-022-00914-8.

52. Wang, D., Wang, X., and Rao, W. (2021). Precise regulation of Ga-based liquid metal oxidation. Acc. Mater. Res. *2*, 1093–1103. https://doi.org/10.1021/accountsmr.1c00173.

53. Li, J., Zhao, X., and Liu, J. (2024). Biosimilar liquid-metal living matter. Matter *7*, 2033–2065. https://doi.org/10.1016/j.matt.2024.04.038.

54. Li, X., Li, M., Shou, Q., Zhou, L., Ge, A., Pei, D., and Li, C. (2020). Liquid metal initiator of ring-opening polymerization: Self-capsulation into thermal/photomoldable powder for multifunctional composites. Adv. Mater. *32*, 2003553. https://doi.org/10.1002/adma.202003553.

55. Matyjaszewski, K., Patten, T.E., and Xia, J. (1997). Controlled/"living" radical polymerization. Kinetics of the homogeneous atom transfer radical polymerization of styrene. J. Am. Chem. Soc. *119*, 674–680. https://doi.org/10.1021/ja963361g.

56. Cabaness, W.R., Lin, T.Y.C., and Párkányi, C. (1971). Effect of pH on the reactivity ratios in the copolymerization of acrylic acid and acrylamide. J. Polym. Sci.: Polym. Chem. *9*, 2155–2170. https://doi.org/10.1002/pol.1971.150090805.

57. Riahinezhad, M., Kazemi, N., McManus, N., and Penlidis, A. (2013). Optimal estimation of reactivity ratios for acrylamide/acrylic acid copolymerization. J. Polym. Sci., Part A: Polym. Chem. *51*, 4819–4827. https://doi.org/10.1002/pola.26906.

58. Du, X., Cui, H., Sun, B., Wang, J., Zhao, Q., Xia, K., Wu, T., and Humayun, M.S. (2017). Photothermally triggered shape-adaptable 3D flexible electronics. Adv. Mater. Technol. *2*, 1700120. https://doi.org/10.1002/admt.201700120.

59. Du, X., Cui, H., Zhao, Q., Wang, J., Chen, H., and Wang, Y. (2019). Inside-out 3D Reversible Ion-Triggered Shape-Morphing Hydrogels. Research *2019*, 6398296.

60. Hu, H., Huang, C., Galluzzi, M., Ye, Q., Xiao, R., Yu, X., and Du, X. (2021). Editing the shape morphing of monocomponent natural polysaccharide hydrogel films. Research *2021*, 9786128.

61. Bagnara, J.T., and Hadley, M.E. (1973). Chromatophores and Color Change: The Comparative Physiology of Animal Pigmentation (Prentice Hall Inc).

62. Jian, N., Guo, R., Zuo, L., Sun, Y., Xue, Y., Liu, J., and Zhang, K. (2023). Bioinspired self-growing hydrogels by harnessing interfacial polymerization. Adv. Mater. *35*, 2210609. https://doi.org/10.1002/adma.202210609.

63. Zhang, J., Liao, J., Liu, Z., Zhang, R., and Sitti, M. (2023). Liquid metal microdroplet-initiated ultra-fast polymerization of a stimuli-responsive hydrogel composite. Adv. Funct. Mater. *34*, 2308238. https://doi.org/10.1002/adfm.202308238.

64. Chaudhuri, O., Cooper-White, J., Janmey, P.A., Mooney, D.J., and Shenoy, V.B. (2020). Effects of extracellular matrix viscoelasticity on cellular behaviour. Nature *584*, 535–546. https://doi.org/10.1038/s41586-020-2612-2.

65. Xi, W., Saw, T.B., Delacour, D., Lim, C.T., and Ladoux, B. (2018). Material approaches to active tissue mechanics. Nat. Rev. Mater. *4*, 23–44. https://doi.org/10.1038/s41578-018-0066-z.

66. Zhao, Q., Wang, J., Wang, Y., Cui, H., and Du, X. (2020). A stage-specific cell-manipulation platform for inducing endothelialization on demand. Natl. Sci. Rev. *7*, 629–643. https://doi.org/10.1093/nsr/nwz188.

67. Zhao, Q., Wang, J., Cui, H., Chen, H., Wang, Y., and Du, X. (2018). Programmed shape-morphing scaffolds enabling facile 3D endothelialization. Adv. Funct. Mater. *28*, 1801027. https://doi.org/10.1002/adfm.201801027.

68. Yi, J., Zou, G., Huang, J., Ren, X., Tian, Q., Yu, Q., Wang, P., Yuan, Y., Tang, W., Wang, C., et al. (2023). Water-responsive supercontractile polymer films for bioelectronic interfaces. Nature *624*, 295–302. https://doi.org/10.1038/s41586-023-06732-y.

69. Kim, E., Jeong, E., Hong, Y.-M., Jeong, I., Kim, J., Kwon, Y.W., Park, Y.-G., Lee, J., Choi, S., Kim, J.-Y., et al. (2025). Magnetically reshapable 3D multi-electrode arrays of liquid metals for electrophysiological analysis of brain organoids. Nat. Commun. *16*, 2011. https://doi.org/10.1038/s41467-024-55752-3.

70. Zhu, X., Wang, F., Zhao, Q., and Du, X. (2024). Adaptive interfacial materials and implants for visual restoration. Adv. Funct. Mater. *34*, 2314575. https://doi.org/10.1002/adfm.202314575.

71. Sheng, H., Liu, R., Li, Q., Lin, Z., He, Y., Blum, T.S., Zhao, H., Tang, X., Wang, W., Jin, L., et al. (2025). Brain implantation of soft bioelectronics via embryonic development. Nature *642*, 954–964. https://doi.org/10.1038/s41586-025-09106-8.

72. Zhu, X., Zhao, Q., Wang, Y., and Du, X. (2026). Multifunctional ferroelectric bioelectronic interfaces for long-term biosafe vagus nerve modulation. Adv. Mater. *38*, e73023. https://doi.org/10.1002/adma.73023.

73. Zhao, Q., Meng, Q., Peng, M., Lu, Z., Liu, Z., Jiang, X., Zheng, H., and Du, X. (2026). A biointegrated living brain stimulator evokes specific neural signalling. Preprint at bioRxiv. https://doi.org/10.64898/2026.05.22.725279.